Active Wireless Sensing for Rapid Information Retrieval in Sensor Networks

Thiagarajan Sivanadyan and Akbar Sayeed *
Department of Electrical and Computer Engineering
University of Wisconsin - Madison
thiagars@cae.wisc.edu, akbar@engr.wisc.edu

ABSTRACT

Most existing information extraction schemes in sensor networks rely on in-network processing that requires information routing and coordination between sensor nodes and incurs a corresponding overhead in delay and energy consumption. In this paper, we propose a viable alternative – Active Wireless Sensing (AWS) – in which a Wireless Information Retriever (WIR) queries a select ensemble of nodes to obtain desired information in a rapid and energy-efficient manner. AWS has two primary attributes: i) the sensor nodes are "dumb" in that they have limited computational ability, and ii) the WIR is computationally powerful, is equipped with an antenna array, and directly interrogates the sensor ensemble with wideband space-time waveforms. AWS is inspired by an intimate connection with communication over multipath channels: the sensor nodes act as active scatterers and produce a multipath response to the WIR's interrogation signals. We develop the basic communication architecture in AWS and explore various signaling and reception strategies at the WIR, and encoding strategies at the sensors. The basic communication architecture is quite flexible and can cater to a variety of information retrieval tasks. In particular, we illustrate the framework in two extreme information retrieval tasks: high-rate information retrieval corresponding to distributed independent sensor measurements, and low-rate retrieval corresponding to localized correlated measurements. A low-complexity interference suppression technique is proposed for significantly increasing the capacity and reliability of high-rate information retrieval. Performance analysis reveals a fundamental rate versus reliability tradeoff in AWS and is illustrated with accompanying simulation results.

Categories and Subject Descriptors

C.2.1 [**Network Architecture and Design**]: Wireless Communication

*This work was partly supported by the NSF under grant CCF 0431088.

IPSN'06, April 19–21, 2006, Nashville, Tennessee, USA.

General Terms

Design, Performance

Keywords

Sensor Networks, Wireless Sensing

1. INTRODUCTION

Existing approaches to information extraction in a wireless sensor network are heavily geared towards in-network processing where either the network as a whole obtains a consistent estimate of desired information (e.g., field data, or some summary statistic), or the distributed information is routed to a decision center via multi-hop routing (see, e.g., [1, 2]). However, in-network processing generally incurs excess delay and energy consumption due to the related tasks of information routing and coordination between nodes. In this paper we propose an alternative approach – Active Wireless Sensing (AWS) — in which a wireless information retriever (WIR) interrogates a select ensemble of sensor nodes for rapid and energy-efficient retrieval of desired information (see Fig. 1). AWS has two primary attributes: i) the sensor nodes are relatively "dumb" in that they have limited computational power, and ii) the WIR is computationally powerful, is equipped with a multi-antenna array, and initiates the information retrieval by interrogating the nodes with wideband space-time waveforms. The

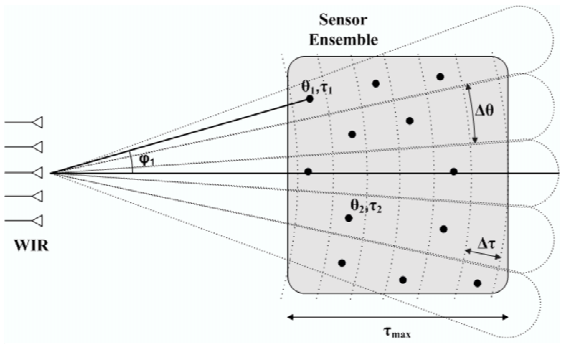

Figure 1: Active Wireless Sensing: basic communication architecture.

basic concept of AWS is inspired by an intimate connection with communication over space-time multiple antenna (MIMO) wireless channels in a multipath environment: sensor nodes act as active scatterers and generate a multipath

signal in response to WIR's interrogation signal. A key idea behind AWS is to separate multiple sensor responses by resolving the multipath signals in angle and delay at a resolution commensurate with the spatio-temporal signal space (see Figs. 1 and 2). This is facilitated by a virtual representation of wideband space-time wireless channels that we have developed in the past several years [5, 6]. In particular, the virtual representation yields a natural partitioning of propagation paths (sensor responses) in angle-delay and provides a mathematical framework for studying fundamental limits of communication over multipath channels at different spatio-temporal resolutions afforded by agile RF front-ends and reconfigurable antenna arrays [7]. Indeed, technological advances in agile RF front-ends provide another motivation for Active Wireless Sensing: WIR's equipped with agile RF transceivers could potentially enable rapid learning of sensor field structure at varying spatio-temporal resolutions. Such WIR's could also be integrated with strategically located access points for network state monitoring and control. AWS is

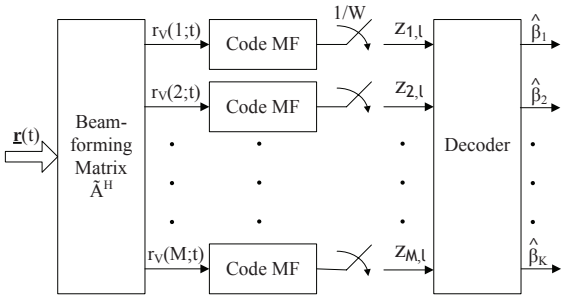

Figure 2: Computation of sufficient statistics at the WIR: angle-delay matched filtering.

similar, in terms of the underlying physics, to the concept of Imaging Sensor Nets that has been independently proposed recently [3, 4]. However, the basic underlying methodology in these works, inspired by radar imaging principles, is quite different and focusses on sensor localization and detection of spatially well-separated events. Our emphasis, in contrast, is on high-rate sensor information retrieval and we exploit connections with recent developments in space-time wireless communications theory. We believe that these two related approaches provide complementary perspectives on information extraction in sensor networks and could be fruitfully cross-leveraged by exploring the connections between wideband radar imaging and wideband wireless communications in the context of sensor networks.

The next section presents the basic space-time communication architecture in AWS by exploiting connections with space-time multipath channels, including sensor encoding strategies and computation of sufficient statistics at the WIR for sensor information retrieval. In Sections 3 and 4 we discuss two extreme sensing configurations involving high-rate information retrieval of multiple independent sensor measurements and low-rate retrieval of multiple correlated sensor measurements, respectively. We also discuss the corresponding processing of the aggregate sensor response at the WIR and analyze the performance of AWS in these cases. Section 5 proposes a low-complexity scheme for mitigating the interference between independent sensor transmissions, thereby significantly increasing the capacity and reliability of information retrieval in AWS. Section 6 presents numerical simulation results to illustrate the performance of AWS in the two sensing configurations and the performance gains due to interference suppression. Section 7 provides a discussion of the results and concluding remarks.

2. THE BASIC SPACE-TIME COMMUNICATION ARCHITECTURE

Consider an ensemble of K sensors uniformly distributed over a region of interest, as illustrated in Fig. 1. We first outline the basic assumptions made in this work. We assume that the WIR, equipped with an M-element array, is sufficiently far from the sensor ensemble, in the same plane, so that far-field assumptions apply. Furthermore, there exists a strong line of sight path between the WIR and each sensor (no fading) and the difference in path loss between individual sensors and the WIR can be neglected due to the large distance between the WIR and the sensor field. The WIR interrogates the sensor ensemble by transmitting wideband (spread-spectrum) signaling waveforms, $\{s_m(t)\}$, from different antennas where each $s_m(t)$ is of duration T and (two-sided) bandwidth W. Let $N = TW \gg 1$ denote the time-bandwidth product of the signaling waveforms that represents the approximate dimension of the temporal signal space. Thus, the signal space of spatio-temporal interrogation waveforms has dimension $MN = MTW$. Certain delay approximations and localization requirements (see Sections 2.1 and 2.2) constrain the bandwidth to: $c/\Delta d < W < 2f_c/M$ where f_c is the carrier frequency, c is the speed of wave propagation, and Δd is the minimum distance between the sensors. The above inequality also implies that $f_c > cM/2\Delta d$. For example, for a sensor separation of $\Delta d = 1$m, a WIR with $M = 10$ antennas uses a signaling bandwidth $W \geq 300$MHz, and a carrier frequency f_c on the order of a few GHz.

2.1 The Multipath Channel in Active Wireless Sensing

We make the practically feasible assumption that the WIR and the sensor nodes are carrier (frequency) synchronized but not phase synchronized. Furthermore, we assume that the phase offset between each sensor and the WIR stays constant at least during the packet duration T. The basic communication protocol consists of the WIR transmitting the space-time signal $\boldsymbol{s}(t) = [s_0(t), s_1(t), \ldots, s_{M-1}(t)]^T$ in an interrogation packet to initiate information retrieval from the sensor ensemble. The i^{th} sensor receives a superposition of the transmitted waveforms

$$x_i(t) = \sum_{\mu=0}^{M-1} s_\mu(t - \tau_{i,\mu}) e^{-j\phi_{i,\mu}} \qquad (1)$$

where $\tau_{i,\mu}$ is the relative (fixed w.r.t. to the antenna in the middle of the array) time-delay between the i^{th} sensor and μ^{th} antenna, $\phi_{i,\mu}$ is the corresponding relative phase offset, and we have assumed that the interrogation packet is transmitted with sufficient power (or is repeated enough) so that the noise in $x_i(t)$ is negligible.

In the far-field, we can choose W so that the relative time delay between the WIR antennas to any sensor is negligible compared to the delay resolution ($\max_\mu \tau_{i,\mu} - \min_\mu \tau_{i,\mu} \ll 1/W$ for all i). This condition translates to a constraint on the carrier frequency, $f_c \gg MW/2$. Under this assumption, the differences in the relative time delays between the

antennas and any sensor can be neglected in the signaling waveform; that is, $s_\mu(t-\tau_{i,\mu}) \approx s_\mu(t-\tau_i)$, for all μ, where τ_i denotes the common delay from the i-th sensor to the WIR. The relative phase offsets in $x_i(t)$ due to different antenna elements $\{\phi_{i,\mu}\}$ consist of a common (random) component ϕ_i and a deterministic component that is captured by the steering/response vector of the array. For simplicity, we consider a one-dimensional uniform linear array (ULA) with spacing d and assume M to be odd WLOG, and define $\tilde{M} = (M-1)/2$. The array steering/response vector for a ULA is given by

$$\boldsymbol{a}(\theta) = \left[e^{j2\pi\tilde{M}\theta}, \ldots, 1, \ldots, e^{-j2\pi\tilde{M}\theta}\right]^T \quad (2)$$

where the normalized angle θ is related to the physical angle of arrival/departure φ (see Fig. 1) as $\theta = d\sin(\varphi)/\lambda$. Here d denotes the distance between the antennas and λ is the wavelength of propagation. The steering/response vector represents the relative phases across antennas for transmitting/receiving a beam in the direction θ. Thus, $x_i(t)$ can be compactly expressed as

$$x_i(t) = e^{-j\phi_i}\boldsymbol{a}^T(\theta_i)\boldsymbol{s}(t-\tau_i) \quad (3)$$

where θ_i denotes the direction of the i-th sensor relative to the WIR array (see Fig. 1). We assume $d = \lambda/2$ spacing, which corresponds to the sensor ensemble projecting maximum angular spread (180 degrees) at the WIR array; larger spacings can be used for smaller angular spreads.[1]

The i-th sensor encodes its measurement in β_i and modulates $x_i(t)$ by β_i and transmits it with energy $\mathcal{E}$ after a fixed duration (same for all sensors) following the reception of the interrogation packet. We assume instantaneous retransmission from each sensor for simplicity. Thus, the transmitted signal from the i-th sensor can be expressed as

$$y_i(t) = \beta_i\sqrt{\frac{\mathcal{E}}{M}}x_i(t) = \beta_i\sqrt{\frac{\mathcal{E}}{M}}e^{-j\phi_i}\boldsymbol{a}^T(\theta_i)\boldsymbol{s}(t-\tau_i) \quad (4)$$

where $E[|\beta_i|^2] = 1$ and $\int E[|x_i(t)|^2]dt = M$ so that $y_i(t)$ has energy $\mathcal{E}$. The received vector signal at the WIR, $\boldsymbol{r}(t) = [r_0(t), r_1(t), \ldots, r_{M-1}(t)]^T$, is a superposition of all sensor transmissions and by the principle of reciprocity it can be expressed as

$$\boldsymbol{r}(t) = \sqrt{\frac{\mathcal{E}}{M}}\sum_{i=1}^{K}\beta_i e^{-j\phi_i}\boldsymbol{a}(\theta_i)\boldsymbol{a}^T(\theta_i)\boldsymbol{s}(t-\tilde{\tau}_i) + \boldsymbol{w}(t) \quad (5)$$

where $\tilde{\tau}_i = 2\tau_i$ denotes the round-trip relative delay in the response from the i^{th} sensor, $\boldsymbol{w}(t)$ denotes an AWGN vector process representing the noise at different WIR antennas, and the random phase ϕ_i includes a random component due to reception at the WIR. Let $\tau_{max} = \max_i \tau_i$ and assume that $\min_i \tau_i = 0$ WLOG. Using (5), the effective system equation relating the received vector signal at the WIR to the transmitted interrogation signal can be expressed as

$$\boldsymbol{r}(t) = \sqrt{\frac{\mathcal{E}}{M}}\int_0^{2\tau_{max}}\boldsymbol{H}(t')\boldsymbol{s}(t-t')dt' + \boldsymbol{w}(t) \quad (6)$$

$$\boldsymbol{H}(t) = \sum_{i=1}^{K}\alpha_i\delta(t-\tilde{\tau}_i)\boldsymbol{a}(\theta_i)\boldsymbol{a}^T(\theta_i) \quad (7)$$

[1] $d = \lambda/2\sin(\varphi_{max})$ spacing results is a one-to-one mapping between $\theta \in [-0.5, 0.5]$ and $\varphi \in [-\varphi_{max}, \varphi_{max}] \subset [-\pi/2, \pi/2]$.

where $\alpha_i = \beta_i e^{-j\phi_i}$, and the $M \times M$ matrix $\boldsymbol{H}(t)$ represents the impulse response for the space-time multipath channel underlying AWS. The delay spread of the channel is $2\tau_{max}$ and we assume that the packet signaling duration $T \gg 2\tau_{max}$.

Note that the above system representation (6), even though it relates the transmitted interrogation signal $\boldsymbol{s}(t)$ to the received signal at the WIR, is independent of the power used for transmitting the interrogation packet. This is because after acquiring the signaling waveform in the interrogation phase, each sensor retransmits it with energy $\mathcal{E}$ and the factor $\sqrt{\mathcal{E}}/\sqrt{M}$ reflects this normalization.

2.2 Sensor Localization Via Multipath Resolution

The active sensing channel matrix (7) has exactly the same form as the impulse response of a physical multiple-antenna (MIMO) multipath wireless channel where the sensor data and phases $\{\alpha_i\}$ in the sensing channel correspond to the complex path gains associated with scattering paths in a MIMO multipath channel [5, 6]. A key motivation of this paper is to leverage insights from communication over multipath MIMO channels in the context of AWS. In particular, we resort to the *virtual representation* of MIMO multipath channels that is a *unitarily equivalent* representation of the physical sensing/multipath channel matrix [5, 6]. A key property of the virtual channel representation is that its coefficients represent a resolution of multipath/sensors in angle and delay (and Doppler in case of relative motion, not considered in this paper) commensurate with the signal space parameters M and W (and T), respectively. The virtual representation in angle corresponds to beamforming in M fixed virtual directions: $\tilde{\theta}_m = m/M$, $m = -\tilde{M}, \cdots, \tilde{M}$. Define the $M \times M$ unitary (DFT) matrix

$$\boldsymbol{A} = \frac{1}{\sqrt{M}}[\boldsymbol{a}(-\tilde{M}/M), \ldots, 1, \ldots, \boldsymbol{a}(\tilde{M}/M)] \quad (8)$$

whose columns are the normalized steering vectors for the virtual angles and form an orthonormal basis for the spatial signal space. The virtual spatial matrix $\boldsymbol{H}_V(t)$ is unitarily equivalent to $\boldsymbol{H}(t)$ as

$$\boldsymbol{H}(t) = \boldsymbol{A}\boldsymbol{H}_V(t)\boldsymbol{A}^T \leftrightarrow \boldsymbol{H}_V(t) = \boldsymbol{A}^H\boldsymbol{H}(t)\boldsymbol{A}^* \quad (9)$$

and the virtual coefficients, representing the coupling between the m-th transmit beam and m'-th receive beam are given by

$$H_V(m', m; t) = \boldsymbol{a}^H(m'/M)\boldsymbol{H}(t)\boldsymbol{a}^*(m/M)/M \quad (10)$$

$$= M\sum_{i=1}^{K}\alpha_i g\left(\theta_i - \frac{m'}{M}\right)g\left(\theta_i - \frac{m}{M}\right)\delta(t-\tilde{\tau}_i) \quad (11)$$

$$\approx H_V(m, m; t)\delta_{m-m'} \quad (12)$$

$$H_V(m, m; t) \approx M\sum_{i\in S_{\theta,m}}\alpha_i g^2\left(\theta_i - \frac{m}{M}\right)\delta(t-\tilde{\tau}_i) \quad (13)$$

where $g(\theta) = \frac{1}{M}\frac{\sin(\pi M\ \theta)}{\sin(\pi\theta)}$ is the Dirichlet sinc function that captures the interaction between the fixed virtual beams and true sensor directions, the last approximation follows from the virtual path partitioning due to beamforming in the virtual representation [5], δ_m denotes the kronecker delta function, and $S_{\theta,m} = \{i \in \{1, \cdots, K\} : -1/2M < \theta_i - m/M \leq$

$1/2M\}$ denotes the set of all sensors whose angles lie in the m-th spatial resolution bin of width $\Delta\theta = 1/M$, centered around the m-th beam. Thus, the virtual spatial representation partitions the sensors in angle: it is approximately diagonal and its m-th diagonal entry contains the superposition of all sensor responses that lie within the m-th beam of width $1/M$.

The sensor responses within each spatial beam can be further partitioned by resolving their delays with resolution $\Delta\tau = 1/W$. Let $L = \lceil 2\tau_{max}W \rceil$ be the largest normalized relative delay. The diagonal entries of virtual spatial matrix can be further decomposed into virtual, uniformly spaced delays as [6]

$$H_V(m,m;t) \approx \sum_{\ell=0}^{L} H_V(m,m,\ell)\delta(t-\ell/W) \tag{14}$$

$$H_V(m,m,\ell) = M\sum_{i=1}^{K} \alpha_i g^2\left(\theta_i - \frac{m}{M}\right)\mathrm{sinc}(W\tilde{\tau}_i - \ell) \tag{15}$$

$$\approx M\sum_{i\in S_{\theta,m}\cap S_{\tau,\ell}} \alpha_i g^2\left(\theta_i - \frac{m}{M}\right)\mathrm{sinc}(W\tilde{\tau}_i - \ell) \tag{16}$$

where $\mathrm{sinc}(x) = \sin(\pi x)/\pi x$ captures the interaction between the fixed virtual and true sensor delays, and $S_{\tau,\ell} = \{i : -1/2W < \tilde{\tau}_i - \ell/W \le 1/2W\}$ is the set of all sensors whose relative delays lie within the ℓ-th delay resolution bin of width $\Delta\tau = 1/W$. Thus, the angle-delay virtual representation partitions the sensor responses into distinct angle-delay resolution bins: the virtual coefficient $H_V(m,m,\ell)$ is a superposition of all sensor responses whose angles and delays lie in the intersection of m-th spatial beam and ℓ-th delay ring (see Fig. 1). For a given number of antennas M and a given minimum spacing between sensors Δd, the bandwidth W can be chosen sufficiently large ($W > c/\Delta d$), in principle, so that there is exactly one sensor in each angle-delay resolution bin (however this is not necessary). In this case, we can define one-to-one mappings $i(m,\ell)$ and $(m(i),\ell(i))$ that associate each sensor with a unique angle-delay resolution bin. It follows from (16) that information retrieval from the i-th sensor amounts to estimating the corresponding virtual angle-delay coefficient

$$\begin{aligned} h_V(m,\ell) &= H_V(m,m,\ell) \leftrightarrow M\beta_{i(m,\ell)}\gamma_{i(m,\ell)} \qquad (17)\\ \gamma_{i(m,\ell)} &= e^{-j\phi_i} g^2(\theta_i - m/M)\mathrm{sinc}(W\tilde{\tau}_i - \ell)|_{i=i(m,\ell)} \ . \end{aligned}$$

2.3 Angle-Delay Sufficient Statistics for Information Retrieval

We now describe the basic processing of the received signal $\boldsymbol{r}(t)$ at the WIR for computing the sufficient statistics for information retrieval, as illustrated in Fig. 2. Define $\boldsymbol{s}(t) = \boldsymbol{A}^*\boldsymbol{s}_V(t)$ and $\boldsymbol{r}_V(t) = \boldsymbol{A}^H\boldsymbol{r}(t)$ where $\boldsymbol{s}_V(t)$ and $\boldsymbol{r}_V(t)$ are the M-dimensional transmitted and received signals in the virtual spatial domain (beamspace). In our model, $\boldsymbol{s}_V(t)$ represents the temporal codes acquired by the sensors in different virtual spatial bins. Using (6), (9) and (14), the system equation (ignoring the fixed delay in re-transmission by the sensor nodes) that relates the received signal to the transmitted signal in the beamspace is

$$\boldsymbol{r}_V(t) = \sqrt{\frac{\mathcal{E}}{M}}\sum_{\ell=0}^{L} \boldsymbol{H}_V(\ell)\boldsymbol{s}_V(t-\ell/W) + \boldsymbol{w}_V(t) \tag{18}$$

where $\boldsymbol{H}_V(\ell)$ represents the virtual spatial matrix corresponding to the ℓ-th virtual delay and $\boldsymbol{w}_V(t)$ represents a vector of independent temporal white AWGN processes with PSD σ^2. Each $\boldsymbol{s}_V(m;t)$, the m-th component of $\boldsymbol{s}_V(t)$, is a unit-energy pseudo-random waveform with bandwidth W and duration T (e.g., a direct-sequence spread spectrum waveform), and we have[2]

$$\langle \boldsymbol{s}_V(m;t-\ell/W), \boldsymbol{s}_V(m;t-\ell'/W)\rangle \approx \delta_{\ell-\ell'} \ . \tag{19}$$

Thus, correlating each $\boldsymbol{r}_V(m;t)$ with delay versions of $\boldsymbol{s}_V(m;t)$ yields the sufficient statistics for information retrieval $\{z_{m,\ell} : m = 1,\cdots,M; \ell = 0,\cdots,L\}$:

$$\begin{aligned} z_{m,\ell} &= \langle \boldsymbol{r}_V(m;t), \boldsymbol{s}_V(m;t-\ell/W)\rangle \qquad (20)\\ &= \int_0^{T+2\tau_{max}} \boldsymbol{r}_V(m,t)\boldsymbol{s}_V^*(m,t-\ell/W)dt. \qquad (21) \end{aligned}$$

Ideal Case: In general, the matched-filter outputs in (21) include the desired response from the sensor in the (m,ℓ)-th angle-delay resolution bin as well as interference from sensors in other resolution bins. Such interference is virtually eliminated in the ideal situation when the sensors positions coincide with the center of the resolution bins; that is, $(\theta_i,\tau_i) = (m/M,\ell/W)$ for some $m \in \{-\tilde{M},\ldots,\tilde{M}\}$ and $\ell \in \{0,\ldots,L-1\}$. In this case, using (17), $\boldsymbol{r}_V(m;t)$ and $z_{m,\ell}$ can be simplified to

$$\begin{aligned} \boldsymbol{r}_V(m;t) \approx& \sqrt{\frac{\mathcal{E}}{M}}\sum_{\ell=0}^{L} h_V(m,\ell)\boldsymbol{s}_V\left(m;t-\frac{\ell}{W}\right)\\ &+w_V(m;t) \qquad (22)\\ z_{m,\ell} \approx& \sqrt{M\mathcal{E}}\beta_{i(m,\ell)}\gamma_{i(m,\ell)} + w_{m,\ell} \ , \qquad (23) \end{aligned}$$

where $\{w_{m,\ell}\}$ are i.i.d. Gaussian with variance σ^2. Note that the factor $\sqrt{M}$ reflects the M-fold array gain or the beamforming gain in reception associated with an M-element antenna array.

2.4 Canonical Sensing Configurations

While different spreading codes can be assigned to different spatial sectors in AWS, in the rest of the paper we focus on an attractive special case in which the same spread-spectrum waveform, $q(t)$ is transmitted on all spatial beams; that is, $s_V(m;t) = q(t)$ for all m. We also assume that we have sufficient angle-delay resolution so that each sensor lies in a unique angle-delay resolution bin. We refer to the $K < ML$ angle-delay resolution bins occupied by transmitting sensors to be "active".[3] The matched filter outputs corresponding to the i-th active sensor can then be uniquely labeled by the by the mapping $z_{(m(i),\ell(i))} \mapsto z_i$ for $i = 1,..,K$. We can now express the matched filter outputs for active bins/sensors as

$$z_i = \sqrt{M\mathcal{E}}\beta_i\tilde{\gamma}_i + \sqrt{M\mathcal{E}}\sum_{k\neq i}\beta_k\tilde{\gamma_{k,i}} + w_i \tag{24}$$

where $\sqrt{M\mathcal{E}}\beta_i\tilde{\gamma}_i$ represents the desired signal component from the i-th sensor and $\beta_k\tilde{\gamma}_{k,i}$, $k \neq i$, represents the in-

[2]The cross-correlation is on the order of $1/N = 1/TW$ and thus very small for large N.

[3]The location of active bins can be reliably determined by the WIR by thresholding the correlator outputs in response to a training interrogation packet. The sensors respond to a training packet with a sufficiently long string of 1's to enhance the receive SNR at the WIR.

terference due to the other $K-1$ active sensors (in other distinct bins) where

$$\tilde{\gamma}_{k,i} = e^{-j\phi_k} g(\theta_k - m(i)/M)\text{sinc}(W\tilde{\tau}_k - \ell(i)) \quad (25)$$

and we note that $\tilde{\gamma}_i = \tilde{\gamma}_{i,i}$. The matched filter outputs $\{z_i = z_{m(i),\ell(i)} : i = 1, \cdots, K\}$ corresponding to the K active angle-delay bins represent the sufficient statistics for information retrieval at the WIR.

In the next two sections, we present two canonical sensing configurations, discuss the corresponding processing at the WIR for desired information retrieval, and analyze the performance of AWS. The two sensing configurations illustrate a rate-reliability tradeoff in AWS. The first case corresponds to high-rate information retrieval, although it comes at the cost of reliability since different sensor transmissions interfere. The second case corresponds to low-rate information retrieval, but it yields higher reliability since multiple sensors transmit the same correlated bit stream and thus do not interfere. In Sec. 5, we present a linear interference suppression schemes for mitigating interference between multiple independent sensor transmissions, which is particularly important for high-rate information retrieval. In all cases, we consider binary transmissions from sensors, for the sake of simplicity. We consider both coherent (BPSK) and non-coherent (on-off) signaling schemes, describe the corresponding receiver processing at the WIR, and analyze the bit-error probability as a function of the transmit power at each sensor. In each configuration, we assume that the exact positions of the sensors are fixed but unknown, i.e. the $\tilde{\gamma}_i$ and $\tilde{\gamma}_{k,i}$ are fixed but unknown.

3. DISTRIBUTED EVENTS: INDEPENDENT SENSOR MEASUREMENTS

This case corresponds to simultaneously sensing multiple spatially distributed events in distinct angle-delay bins. We assume that the K sensor measurements for distinct events are independent and the sensors encode their measurements in a binary data stream. Thus, the transmitted bit streams are independent across sensors, and for simplicity we also assume that each sensor's bit stream is independent across time. This case represents high-rate information retrieval and a total of K bits are retrieved by the WIR during each transmission interval.

3.1 Coherent Signaling

The sensors employ BPSK modulation, $\{\beta_i \in \{-1, +1\}\}$, and the phases $\{\phi_i\}$ are known (or estimated) at the receiver. In this case, we assume that the phases $\{\phi_i\}$ are stable for at least two transmission intervals. Each sensor transmission consists of two packets: a training packet of '+1' for phase estimation at the WIR followed by an information packet. Assuming perfect phase estimate at the WIR (performance with estimated phases is illustrated in Sec. 6), the phase corrected matched filter output for the i-th active bin is given by

$$\begin{aligned} \tilde{z}_i &= e^{j\phi_i} z_i & (26)\\ &= \sqrt{M\mathcal{E}}\beta_i|\tilde{\gamma}_i| + \sqrt{M\mathcal{E}}\sum_{k\neq i}\beta_k\tilde{\gamma}_{k,i}e^{j\phi_i} + w_i & (27)\\ &= S_i + I_i + w_i & (28) \end{aligned}$$

where S_i and I_i represent the signal and interference terms, respectively. Using the Gaussian approximation for the interference I_i [8], the optimal estimate for the i^{th} sensor transmission is $\hat{\beta}_i = \text{sign}\{Re(\tilde{z}_i)\}$. The probability of error is characterized by the the Signal-to-Interference-and-Noise-Ratio (SINR) [8, 9]

$$P_e = Q\left(\sqrt{SINR}\right) = Q\left(\sqrt{\frac{2M|\tilde{\gamma}_i|^2\mathcal{E}}{\sigma^2 + M\sum_{k\neq i}|\tilde{\gamma}_{k,i}|^2\mathcal{E}}}\right) \quad (29)$$

where the signal power $E[|S_i|^2] = M|\tilde{\gamma}_i|^2\mathcal{E}$, the interference power $E[|I_i|^2] = M\sum_{k\neq i}|\tilde{\gamma}_{k,i}|^2\mathcal{E}$ and σ^2 denotes the variance of AWGN w_i. We note that the system is interference limited and thus P_e exhibits an error floor in the limit of high SNR

$$P_e \to Q\left(\sqrt{\frac{2|\tilde{\gamma}_i|^2}{\sum_{k\neq i}|\tilde{\gamma}_{k,i}|^2}}\right) \quad (30)$$

which is a function only of the number of sensors and the sensor positions. In the ideal case, if the sensor positions are exactly aligned with the center of the angle-delay resolution bins, then $\tilde{\gamma}_{k,i} = \delta_{k-i}$. In this case, there is no interference between sensors and the P_e is given by

$$P_e = Q\left(\sqrt{\frac{2M\mathcal{E}}{\sigma^2}}\right) \quad (31)$$

which is the well-known P_e for antipodal signaling over AWGN channels and reflects the M-fold increase in the received SNR at the WIR due to array gain.

3.2 Non-Coherent Signaling

The sensors employ non-coherent (on-off) signaling, $\beta_i \in \{0, \sqrt{2}\}$, and the ϕ_i are assumed unknown at the WIR. In this case, the matched filter output in (24) takes the form

$$\begin{aligned} H_0 &: z_i = I_i + w_i & (32)\\ H_1 &: z_i = S_i + I_i + w_i & (33) \end{aligned}$$

where $S_i = \sqrt{2M\mathcal{E}}\beta_i\tilde{\gamma}_i$ and $I_i = \sqrt{2M\mathcal{E}}\sum_{k\neq i}\beta_k\tilde{\gamma}_{k,i}$ represent the signal and interference components, respectively. Again, approximating interference as Gaussian [8] and using standard techniques [9], the optimal decision takes the form

$$\frac{p(z_i|H_1)}{p(z_i|H_0)} \gtrless 1 \Rightarrow \boldsymbol{I_0}\left(\frac{2\alpha|z_i|}{\tilde{\sigma}^2}\right) \gtrless e^{\alpha^2/\tilde{\sigma}^2} \quad (34)$$

where $\alpha = \sqrt{2M\mathcal{E}}|\tilde{\gamma}_i|$, $\tilde{\sigma}^2 = 2M\sum_{k\neq i}|\tilde{\gamma}_{k,i}|^2\mathcal{E} + \sigma^2$, and $\boldsymbol{I_0}$ is the modified Bessel function of type 1 and order 0. Due to monotonicity of $\boldsymbol{I_0}$, the optimum detection rule simplifies to $|z_i| \gtrless \lambda$. The optimal threshold λ is a function of $\tilde{\gamma}_i$ and $\tilde{\sigma}^2$, and can be optimized for a particular network set up. The P_e can be characterized by noting that $|z_i|$ is Rayleigh under H_0 and Rician H_1:

$$\begin{aligned} P_e &= \frac{1}{2}\left[P_{e,0} + P_{e,1}\right] & (35)\\ P_{e,0} &= P(|z_i| > \lambda|H_0) = e^{-\lambda^2/\tilde{\sigma}^2} & (36)\\ P_{e,1} &= P(|z_i| < \lambda|H_1) = F_{\chi_2'^2(\frac{2\alpha^2}{\sigma^2})}\left(\frac{2\lambda^2}{\tilde{\sigma}^2}\right) & (37) \end{aligned}$$

where $F_{\chi_2'^2(x)}(y)$ is the distribution function of a non-central chi-squared random variable with non-centrality parameter x and 2 degrees of freedom.

In the ideal case, since $\tilde{\gamma}_{ki} = \delta_{k-i}$, we have $\alpha^2 = 2M\mathcal{E}$ and $\tilde{\sigma}^2 = \sigma^2$ and the P_e becomes

$$P_e = \frac{1}{2}e^{-\lambda^2/\sigma^2} + \frac{1}{2}F_{\chi_2'^2(\frac{4M\mathcal{E}}{\sigma^2})}\left(\frac{2\lambda^2}{\sigma^2}\right) \quad (38)$$

which is the P_e for a on-off signaling with unknown random phase, and the factor M in the non-centrality parameter reflects the array gain.

4. LOCALIZED EVENT: CORRELATED SENSOR MEASUREMENTS

This case corresponds to sensing a single localized event by sensors in multiple adjacent angle-delay bins. We assume that the sensor measurements are highly correlated (redundant sensing) and we abstract it by assuming that all sensors transmit identical bit streams; that is, $\beta_i = \beta$ for all i. However, we assume that the common transmitted bit is independent in different transmission intervals.

4.1 Coherent Signaling

The optimal decision in this case is based on the sum of phase-corrected MF outputs, $\hat{\beta} = \text{sign}(Re(\sum \tilde{z}_i))$ where

$$\tilde{z}_i = z_i e^{j\phi_i} = \sqrt{M\mathcal{E}}\beta\left(|\tilde{\gamma}_i| + \sum_{k\neq i}\tilde{\gamma}_{ki}e^{j\phi_i}\right) + \tilde{w}_i. \quad (39)$$

The corresponding error probability is approximately given by

$$P_e = Q\left(\sqrt{\frac{2M\mathcal{E}(\sum_i|\tilde{\gamma}_i|^2 + (1/2)\sum_i\sum_{k\neq i}|\tilde{\gamma}_{k,i}|^2)}{\sigma^2}}\right). \quad (40)$$

Thus we get a K fold SNR increase compared to the case of independent transmissions since different sensors instead of interfering contribute to each bit. In the ideal case, the K sensors' transmissions are essentially K parallel AWGN channels transmitting the same data and

$$P_e = Q\left(\sqrt{\frac{2MK\mathcal{E}}{\sigma^2}}\right) \quad (41)$$

which is the P_e for a BPSK signaling system transmitting with K times the individual sensor power.

4.2 Non-Coherent Signaling

With identical on-off transmissions from the sensors, the MF outputs for the K active sensor bins can be simplified to $z_i = \alpha_i + w_i$ where $\alpha_i = \sqrt{2M\mathcal{E}}(\tilde{\gamma}_i + \sum_{k\neq i}\tilde{\gamma}_{k,i})$ represents the effective signal strength. Solving the joint detection problem for β and replicating the procedure followed in Sec. 3.2 one can obtain the optimal decision

$$\hat{\beta} = \text{sign}\left(\sum_i |z_i|^2 - \lambda^2\right) \quad (42)$$

where λ^2 is the optimal threshold that can be optimized for a given network configuration. Note that $|z_i||H_0 \sim$ Rayleigh$(\sigma^2/2)$ and hence $(2/\sigma^2)|z_i|^2|H_0 \sim \chi^2_2$, the standard central chi-squared distribution with 2 degrees of freedom. Thus,

$$P_{e,0} = P\left(\sum_i |z_i|^2 < \lambda^2|H_0\right) = 1 - F_{\chi^2_{2K}}\left(\frac{2\lambda^2}{\sigma^2}\right) \quad (43)$$

where $F_{\chi^2_{2K}}(x)$ is the distribution function of a central chi-squared random variable with $2K$ degrees of freedom.

Under H_1, $|z_i||H_1 \sim$ Rice$(|\alpha_i|^2, \sigma^2/2)$ which results in $\frac{2}{\sigma^2}\sum_i|z_i|^2|H_1 \sim \chi'^2_{2K}(2\alpha^2/\sigma^2)$ where $\alpha^2 = \sum_i|\alpha_i|^2$. Thus, $P_{e,1} = P(\sum_i|z_i|^2 < \lambda^2|H_1)$ can be given in terms of the cdf of the chi-squared distribution, and the resulting P_e is

$$P_e = \frac{1}{2}\left[1 - F_{\chi^2_{2K}}\left(\frac{2\lambda^2}{\sigma^2}\right)\right] + \frac{1}{2}F_{\chi'^2_{2K}(\frac{2\alpha^2}{\sigma^2})}\left(\frac{2\lambda^2}{\sigma^2}\right) \quad (44)$$

Compared to the independent transmissions case, the absence of interference in the K parallel transmissions yields significant performance improvements. In the ideal situation, we have $\alpha^2 = 2KM\mathcal{E}$ and hence

$$P_e = \frac{1}{2}\left[1 - F_{\chi^2_{2K}}\left(\frac{2\lambda^2}{\sigma^2}\right)\right] + \frac{1}{2}F_{\chi'^2_{2K}(\frac{4KM\mathcal{E}}{\sigma^2})}\left(\frac{2\lambda^2}{\sigma^2}\right). \quad (45)$$

5. SUPPRESSING INTERFERENCE BETWEEN INDEPENDENT SENSOR TRANSMISSIONS

Retrieval of independent data streams from active sensors is the most challenging information retrieval task from a communication viewpoint due to interference between sensor transmissions. This is particularly true when a large number of sensors are active. As we discussed in Sec. 3 (and as illustrated by numerical results in Sec. 6), P_e of detection based on angle-delay matched filter outputs suffers from an error floor as the sensor transmission power is increased. Thus, methods for mitigating inter-sensor interference are critical for energy-efficient operation in AWS. The low-power communication channel from the sensor network to the WIR is a multiple access channel and the different sensors are analogous to multiple users simultaneously accessing the channel. Thus, a range of multiuser detection techniques [8] can be leveraged in this context. It is well-known that the optimum multiuser detector suffers from exponential complexity in the number of users/sensors. However, low-complexity linear interference suppression techniques can yield competitive performance [8]. In this section, we describe a simple linear interference suppression technique based on the idea of linearly constrained minimum variance (LCMV) filtering [8, 11] that yields impressive performance gains over simple matched filtering, as illustrated by numerical results in Sec. 6.

The basic idea behind LCMV is to exploit the correlation between the interference corrupting the MF output of a desired active angle-delay bin and the MF outputs of the remaining active bins to suppress the interference in the desired MF output. This is attained by designing K LCMV filters for the active angle-delay bins that jointly operate on all active MF outputs. The filters operate on the MF outputs within each transmission interval; no joint processing is done across multiple transmissions in time. Let $\boldsymbol{z} = [z_1 \dots z_K]^T$ denote the vector of MF outputs corresponding to the active sensors/angle-delay bins. Using (24), it takes the form

$$\boldsymbol{z} = \boldsymbol{\Gamma}\boldsymbol{\beta} + \boldsymbol{w} \quad (46)$$

where $\boldsymbol{\Gamma} = [\boldsymbol{\Gamma}_{i,j}] = [\tilde{\gamma}_{j,i}]$ is the coupling matrix between the K sensors, $\boldsymbol{\beta} = [\beta_1 \dots \beta_K]^T$ is the vector of sensor data and $\boldsymbol{w}$ is a complex AWGN vector with variance σ^2. The filtered sufficient statistic $\hat{z}_i$ for the i^{th} sensor is obtained as $\hat{z}_i = \boldsymbol{h}^H_{i,opt}\boldsymbol{z}$, and the filter $\boldsymbol{h}_{i,opt}$ is designed to minimize the

output power (variance) of $\hat{z}_i$ subject to a linear constraint that preserves the desired signal from the i-th sensor:

$$\boldsymbol{h}_{i,opt} = \arg\min E[|\boldsymbol{h}^H \boldsymbol{z}|^2] \;\text{ s.t. }\; \boldsymbol{h}^H \Gamma_i = 1 \qquad (47)$$

where Γ_i is the i^{th} column of $\boldsymbol{\Gamma}$. The optimum filter is given by [11]

$$\boldsymbol{h}_{i,opt} = \frac{\boldsymbol{R}^{-1}\Gamma_i}{\Gamma_i^H \boldsymbol{R}^{-1}\Gamma_i} \qquad (48)$$

where $\boldsymbol{R} = E[\boldsymbol{z}\boldsymbol{z}^H]$ is the correlation matrix of the active MF outputs. In essence, the constrained optimization results in reduction of interference power in the filter MF output $\tilde{z}_i$, while preserving the desired signal from the i-th sensor. The final bit decisions are made based on the filtered MF outputs $\{\tilde{z}_i\}$ as described in Sec. 3 for both coherent and non-coherent transmissions. Similarly, the corresponding P_e can be estimating by computing the signal power and the residual interference power in $\{\tilde{z}_i\}$ [8]. We omit the details due to lack of space. We note that the P_e associated with LCMV filtering does not suffer from error floors [8] as confirmed by the numerical results presented in the next section.

The computation of LCMV filters can be done in a variety of ways, in practice. The data correlation matrix $\boldsymbol{R}$ can be directly estimated by using MF outputs for multiple transmission periods. The estimation of the coupling matrix, Γ, which defines the constraints, is more challenging. One approach is to make different sensors transmit in disjoint transmission intervals from which different columns of Γ can be estimated. Alternatively, finer angle-delay position estimates for the different active sensors could be obtained by oversampling the matched filtered outputs in angle and delay. Then, an approximation to the coupling matrix could be obtained via the analytical expressions for $\tilde{\gamma}_{k,i}$ (see (25)).

6. NUMERICAL RESULTS

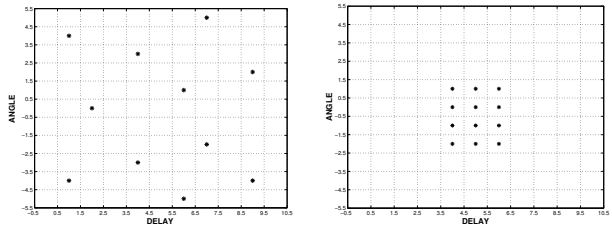

(a) (b)

Figure 3: Angle-delay resolution bins for active sensors. (a) Independent measurements for multiple distributed events. (b) Correlated measurements for a localized event.

A single spread-spectrum waveform is used for all virtual spatial beams: $s_V(m;t) = q(t)$ for all m, where a length $N = TW = 127$ pseudo-random binary code is used for $q(t)$. For coherent reception, we assume that the phases $\{\phi_i\}$ remain constant over two transmission intervals and each sensor transmits two bits for each information bit: a training bit from which the WIR estimates its relative phase, followed by the information bit. We consider $M = L = 11$ corresponding to a total of $ML = 121$ angle-delay resolution bins.

We first illustrate the performance of AWS in the two extreme sensing configurations discussed earlier and depicted in Fig. 3. The configuration corresponding to distributed independent events (Sec. 3) is depicted in Fig. 3(a) and represents independent sensor transmissions from $K = 11$ distinct bins. The transmission bits are i.i.d. across sensors as well as across time and thus a total of 11 bits are retrieved in each transmission interval. The probability of error P_e as a function of the transmit SNR (per sensor) is shown in Fig. 4(a) for both coherent and non-coherent transmissions. The ideal non-coherent and coherent curves represent benchmarks in which the sensors are located at the center of the bins to minimize interference. All other P_e (non-ideal) plots correspond to a random but fixed position of sensors within their respective bins, and the P_e reflects the average performance across all active sensors. Non-ideal, non-coherent detection incurs a loss in SNR and also exhibits a P_e floor of $\approx 2 \times 10^{-5}$ around 15dB due to interference. Remarkably, coherent detection performs quite well even in the presence of interference and for training SNR as low as 0dB.

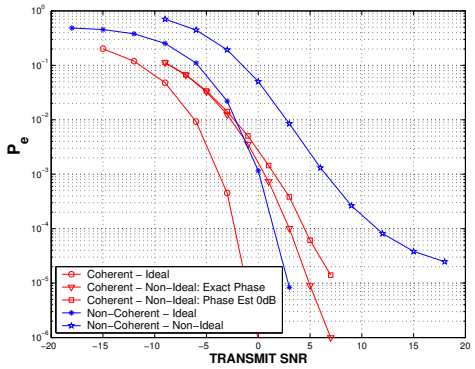

(a)

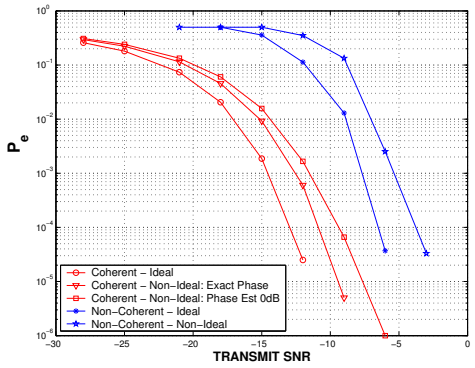

(b)

Figure 4: P_e vs. SNR plots. (a) Independent sensor transmissions. 11 bits per transmission. (b) Identical sensor transmissions. 1 bit per transmission.

The sensing configuration corresponding to correlated (redundant) sensing of a localized event (Sec. 4) is depicted in Fig. 3(b) and represents identical transmissions from $K = 12$ adjacent bins. Thus, a single bit of information is retrieved in each transmission period. As expected from our analysis in Sec. 4, this case exhibits a dramatic improvement in P_e compared to independent transmissions due to lack of interference (see Fig. 4(b)); in fact, it yields an SNR gain proportional to K due to identical transmissions. Non-ideal

detectors (both coherent and non-coherent) perform nearly as well as ideal detection (no error floors) and coherent detection shows about 7dB gain over non-coherent detection.

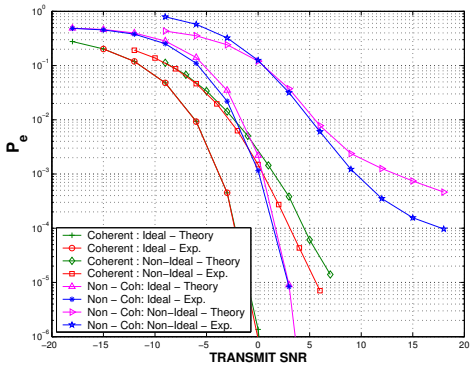

Figure 5: Comparison of analytical P_e calculations with numerical results.

Fig. 5 compares the experimental P_e plots in Fig. 4 with the analytic expressions obtained in Sections 3 and 4. As expected, the agreement is excellent for the ideal curves. The agreement is quite good even for the non-ideal plots and the deviations can be attributed due to the Gaussian approximation of interference (as also noted in [8]).

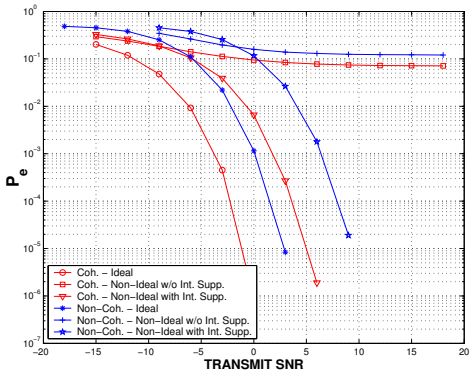

Figure 6: P_e versus SNR plot for high-rate information retrieval with interference suppression. 121 bits per transmission.

Finally, Fig. 6 illustrates the performance of high-rate information retrieval with interference suppression (Sec. 5) in the extreme case when all available $ML = 121$ angle-delay bins are active (corresponding to all bins in Fig. 3(a) being active) and the active sensors send independent bit streams. In this case, 121 bits are retrieved in each transmission interval. As evident from Fig. 6, which represents the P_e for a sensor near the center of the angle-delay grid (maximum interference), AWS with interference suppression delivers remarkable performance and exhibits no error floors in contrast to MF-based detection.

7. DISCUSSION AND CONCLUSIONS

Active Wireless Sensing (AWS) exploits MTW signal space dimensions in time, frequency and space for rapid and energy-efficient information retrieval from a sensor ensemble. In effect, a maximum of ML ($L \ll TW$) channels can be established for information retrieval by resolving sensors in angle and delay via angle-delay matched filtering, which also gives a sensor localization map at a resolution commensurate with M and W.

The numerical results illustrate an inherent rate-reliability tradeoff in AWS. The rate of information retrieval can be increased by sensing independent distributed events through $N_c < ML$ sensing channels, although at the cost of reliability due to interference between sensor transmissions. On the other hand, reliability can be dramatically increased by using all N_c channels for redundant localized sensing at the cost of rate. The use of low-complexity linear interference techniques at the WIR significantly enhances the capacity and reliability of information retrieval in AWS.

There are many exciting avenues for future work. First, it is not necessary to resolve a single sensor in each angle-delay bin. In fact, multiple correlated sensor transmissions from within each resolution bin could be exploited for dramatic reduction in power consumption via phase-coherent transmissions [12]. Furthermore, the sensor power consumption can be further reduced significantly by using independently coded transmissions from different sensors. Overall, AWS offers a range of strategies for optimizing the rate-reliability tradeoff and energy efficiency in a given sensing task. Ultimately, our goal is to leverage AWS at multiple spatio-temporal resolutions to rapidly learn the salient spatio-temporal structures in the sensor field.

8. REFERENCES

[1] D. Estrin, L. Girod, G. Pottie and M. Srivastava, "Instrumenting the world with wireless sensor networks," *Proc. ICASSP 2001.*

[2] *IEEE J. Select. Areas Commun.*, Special Issues on Sensor Networks, August 2004, April 2005.

[3] B. Ananthasubramaniam and U. Madhow, "Virtual Radar Imaging for Sensor Networks", *Proc. IPSN 2004.*

[4] B. Ananthasubramaniam and U. Madhow, "Detection and Localization of Events in Imaging Sensor Nets", *Proc. IEEE ISIT 2005.*

[5] A. Sayeed, "Deconstructing Multi-antenna Fading Channels", *IEEE Trans. on Signal Processing*, Oct. 2002.

[6] A. Sayeed, "A Virtual Representation for Time- and Frequency-Selective Correlated MIMO Channels," *Proc. IEEE ICASSP 2003.*

[7] A. Sayeed, V. Raghavan, and J. Kotecha, "Capacity of Space-Time Wireless Channels: A Physical Perspective," *Proc. IEEE ITW 2004.*

[8] S. Verdu, *Multiuser Detection*, Cambridge University Press.

[9] J. Proakis, *Digital Communications*, 3rd Ed., Prentice Hall.

[10] S. M. Kay, *Fundamentals of Statistical Signal Processing: Detection Theory*, Prentice Hall.

[11] S. Haykin, *Adaptive Filter Theory*, 4th Ed., Prentice Hall.

[12] W. Bajwa, A. Sayeed, and R. Nowak, "Matched Source-Channel Communication for Field Estimation in Wireless Sensor Networks," *Proc. IPSN 2005.*